Experimental Electron Density Studies for Investigating the Metal π-Ligand Bond: the Case of Bis(1,5-cyclooctadiene)nickel

Piero Macchi,* Davide M. Proserpio, and Angelo Sironi*

Contribution from the Dipartimento di Chimica Strutturale e Stereochimica Inorganica, Via Venezian 21, 20133 Milano, Italy

Received July 28, 1997

Abstract: The accurate experimental electron density of crystalline bis(5-cyclooctadiene)nickel, $Ni(COD)_2$, has been determined by X-ray diffraction ($T = 125$ K, 17 051 reflections measured for $2\theta \leq 96°$) and it has been interpreted in terms of quantum theory of atoms in molecules (QTAM). The data were measured with a CCD area detector, whose performances were tested. This experimental electron density study of a π-ligand η^2-coordinated to a metal atom is intended to test the Dewar−Chatt−Duncanson (DCD) bonding formalism providing further information about the π-complex vs metallacycle dichotomy. QTAM analysis, within the NiC_2 triangle, shows a ring structure with a bond critical point between the two $C(sp^2)$, two bond critical points between Ni and each carbon, and one ring critical point in its center. Topology speaks for a π-complex with a *concave* ring structure and the overall bonding picture is in agreement with the DCD model: σ-donation and π-back-bonding are recognized in the Ni−C bond paths, which are *inwardly* curved (σ-donation) but well separated (π-back-donation).

Introduction

Accurate experimental electron density (ED) studies have become, in the last three decades, a powerful tool for bonding analysis providing superior information on the nature of chemical bond itself.[1a] In particular, the successful application of Bader's quantum theory of atoms in molecules (QTAM)[1b] to the experimentally determined $\rho(\mathbf{r})$ has been the most important step in the coupling of X-ray studies and theoretical chemistry. Historically, the main field studied was that of small organic molecular crystals and, more recently, that of biological or pharmacological compounds.[2] While a few transition metal complexes were investigated early on,[3] recently there has been a resurgence of interest in this area,[4] but only a few molecules involving organometallic bonds have been considered so far.

This paper reports on the determination of the accurate ED of crystalline bis(1,5-cyclooctadiene)Nickel, $Ni(COD)_2$, by X-ray diffraction (125 K, $2\theta \leq 96°$) and its interpretation in terms of QTAM. This is the first experimental electron density study of a π-ligand η^2-coordinated to a metal atom[5] and it should allow an 'experimental test' of the Dewar−Chatt−Duncanson (DCD)[6] bonding formalism and provide information concerning the π-complex vs metallacycle dichotomy.

Intensities were collected on a Siemens SMART CCD area detector diffractometer, whose adequacy was initially tested by recollecting (at 120 K), on a reference crystal, a dataset previously measured with a conventional detector at lower temperature (18 K).[7] This kind of area detector allows very fast data collection (80 h for $Ni(COD)_2$) without loss of accuracy; a feature which is particularly useful when dealing with crystal decay (4.5% in the present case), which is time dependent.

Atomic positions were accurately determined within the conventional neutral independent atom model (IAM) and the aspherical atom formalism was then applied to obtain detailed information about electron deformation density. A complete topological analysis of $\rho(\mathbf{r})$ was performed with a careful description of the M-(η^2-C_2) π-bond regions. Experimental Ni d-orbital occupancies were determined and related to the overall bonding picture by means of extended Hückel (EHT) molecular

* Address correspondence to this author. E-mail: angelo@csmtbo.mi.cnr.it.

(1) (a) Coppens, P. *X-Ray charge densities and chemical bonding*. IUCr Texts on Crystallography, Oxford University Press: Oxford, 1997. (b) Bader, R. F. W. *Atoms in molecules: a quantum theory*. **1990**, International series of monographs on chemistry, *22* (Oxford). These two books contain most of the theoretical background for applications of experimental ED determination and QTAM analysis; all references cited hereafter address, however, the original papers which deal with the specific arguments discussed.

(2) (a) Chen, L.; Craven, B. *Acta Crystallogr.* **1995**, *B51*, 1081−1097. (b) Howard, S.; Hursthouse, M.; Lehmann, C.; Poyner, E. *Acta Crystallogr.* **1995**, *B51*, 328−337. (c) Pichon-Pesme, V.; Lecomte, C.; Lachekar, H. *J. Phys. Chem.* **1995**, *99*, 6242−6250. (d) Roversi, P.; Barzaghi, M.; Merati, F.; Destro, R. *Can. J. Chem.* **1996**, *74*, 1145−1161. (e) Roversi, P. *Ph.D. Thesis*, Milano, Italy, **1996**, 66−107.

(3) See, for instance: (a) Rees, B.; Coppens, P. *Acta Crystallogr.* **1973**, *B29*, 2516−2527. (b) Rees, B.; Mitschler, A. *J. Am. Chem. Soc.* **1976**, *98*, 7918−7924. (c) Nielsen, F. S.; Lee, P.; Coppens, P. *Acta Crystallogr.* **1986**, 359−364.

(4) (a) Bianchi, R.; Gatti, C.; Adovasio, V.; Nardelli, M. *Acta Crystallogr.* **1996**, *B52*, 471−478. (b) Iversen, B. B.; Larsen, F. K.; Figgis, B. N.; Reynolds, P. A.; Schultz, A. J. *Acta Crystallogr.* **1996**, *B52*, 923−931. (c) Antipin, M. Y.; Lyssenko, K.; Boese, R. *J. Organomet. Chem.* **1996**, *508*, 259−262. (d) Bolotovsky, R.; Darovsky, A.; Kezerashvili, V.; Coppens, P. *J. Synchr. Rad.* **1995**, *28*, 86−88. (e) Lee, C. S.; Hwang, T. S.; Wang, Y.; Peng, S. M.; Hwang, C. S. *J. Phys. Chem.* **1996**, *100*, 2934−2941. (f) Smith, G. T.; Mallinson, P. R.; Frampton, C. S.; Farrugia, L. J.; Peacock, R. D.; Howard, J. A. K. *J. Am. Chem. Soc.* **1997**, *119*, 5028−5034. (g) Iversen, B. B.; Larsen, F. K.; Figgis, B. N.; Reynolds, P. A. *J. Chem. Soc., Dalton Trans.* **1997**, 2227−2240.

(5) References 3a, 3b, and 4c deal with η^5 and η^6 delocalized π-systems coordinated to a transition metal atoms. Moreover, a QTAM analysis has not been performed in these works.

(6) (a) Dewar, J. S. *Bull. Soc. Chim. Fr.* **1951**, *18*, C71. (b) Chatt. J.; Duncanson, L. A. *J. Chem. Soc.* **1953**, 2939−2947.

(7) The test has been performed on 2-[(4-butyl-2-methyl-6-oxo-5-{4-[2-(1*H*-tetrazol-5yl)phenyl]benzyl}-1*H*-pyrimidin-1-yl)methyl]-3-thiophenecarboxylate (LR-B/081), a pharmacological compound. See: (a) Destro, R.; Soave, R. *Acta Crystallogr.* **1995**, *C51*, 1383−1385 for its room temperature geometry; a complete report of this test is in press [(b) Macchi, P.; Proserpio, D. M.; Sironi, A.; Soave, R.; Destro, R. *J. Appl. Crystallogr.*] and a short description is here added as Supporting Information. We thank Prof. R. Destro, Dr. P. Roversi, and Dr. R. Soave for kindly supplying a few low-temperature data sets for this (and other) tests.

S0002-7863(97)02558-4 CCC: $15.00
Published on Web 02/10/1998

Table 1. Crystal Data for $Ni(COD)_2$

chemical formula	$C_{16}H_{24}Ni$	total reflectns (redundancy)	17051 (1.16)
a	7.370(1) Å		
b	9.092(1) Å	unique reflectns (R_{int})	9612 (0.0144)
c	10.758(1) Å	R_σ	0.0296
α	71.85(1)°	μ	1.49 mm^{-1}
β	84.27(1)°	ρ_{calcd}	1.423 g/cm^3
γ	69.58(2)°	scan method	*ω*
V	641.9(1) $Å^3$	frame width	0.3°
Z	2	time per frame	90 s
crystal system	triclinic	no. of frames	2600
space group	$P\bar{1}$	detector−sample distance	3.95 cm
T	125 K		

orbital calculations which were also used to compute bond orders later compared with their experimental counterparts.

Experimental Section

When dealing with accurate electron density determination, the sample and the experimental conditions must be chosen in order to minimize *post-hoc* corrections and a large set of high quality X-ray reflections is required to reduce correlation effects and uncertainties of nuclear positions (on which the pseudoatom multipolar expansions are centered). In this context, the choice of $Ni(COD)_2$ gave some undoubted advantages: (i) absorption effects, which hold great importance when the compound contains heavy atoms, are limited (Ni being a first transition metal); (ii) the ratio n_v/n_c (n_v = number of valence electrons; n_c = number of core electrons) is favorably high,[8] ensuring that aspherical distribution accounts for a larger variance; (iii) the small cell volume allows to set a short detector-to-sample distance, hence to reduce the overall time collection while enhancing the counting statistics reflection intensities.[9] Luckily, the crystal showed also a good scattering power even at high 2θ angles and a large set of accurately determined data was eventually available.

Data Collection. A pale yellow triangular prism of $Ni(COD)_2$ 0.20 × 0.20 × 0.10 mm was mounted on a glass fiber in N_2 atmosphere on a Siemens SMART CCD area detector diffractometer. Graphite-monochromatized Mo Kα (λ = 0.710 73 Å) radiation was used with generator working at 50 kV and 35 mA.[10] The sample was cooled to 125 K in 3 h with a mean temperature gradient of −1 K/min. The glass fiber was short enough to keep a contact between the N_2 flow and the metal pin (thus avoiding the icing of the crystal). During sample cooling, cell parameters were controlled to have a monitoring of the phase stability. Cell parameters and orientation matrix were initially determined from least-squares refinement on 63 reflections measured in two different sets of 15 frames each, in the range $0 < \theta < 30°$. At 125 K the cell volume resulted ca. 1.5% smaller than that at room temperature. Crystal data for $Ni(COD)_2$ are reported in Table 1.

The intensities were collected with ω-scan technique ($\Delta\omega = 0.3°$) within the limits $0 < 2\theta < 96°$ (maximum $\sin\theta/\lambda = 1.05$ $Å^{-1}$). The short distance detector−sample (=3.95 cm) allowed a fast data-collection strategy: (a) two sets (of 650 frames each), 90 s *per* frame, detector arm at $\theta = 35°$, ϕ= 0, 180°, $2\theta_{max} = 70°$; (b) two sets (of 650 frames each), 90 s *per* frame, detector arm at $\theta = 65°$, ϕ= 90, 270°, $2\theta_{min} = 30°$, $2\theta_{max} = 96°$.[11]

The first 50 frames, containing 163 reflections (in the range $0 < 2\theta < 60°$) were recollected at the end to estimate the overall crystal decay (4.5%), whose correction was applied together with that for absorption (SADABS).

Determination of the Molecular Geometry. A first spherical atom refinement (SHELX93)[12] was carried out, starting from the published data[13] after reducing the unit cell. The 9369 unique reflections with $I/\sigma(I) > 0$ were used (weighting: $w = 1/[\sigma^2(F_o2) + (0.0220(F_o2 + 2F_c2)/3)^2]$); anisotropic temperature factors were assigned to all non-hydrogen atoms. Hydrogen positional parameters were finally included (without constraints) in the refinement together with their isotropic thermal factors (model **1**).

Model **1** was improved determining heavy atom positions by a *high order* refinement ($2\theta > 70°$). Then, all data available were employed to accurately determine positional parameters for H atoms, refined by using generalized scattering factors (GSF) for H_2 molecule polarized in the direction of the bonded C atom, including monopole (model **2a**)[14] and dipole terms (model **2b**);[15] in both refinements $w = 1/\sigma(F^2)$ was used. Note that, in models **1** and **2a,** the mean C−H distance[16] was 0.97(2) and 0.98(2) Å respectively, while in model **2b** a more realistic averaged value, 1.09(2) Å, was obtained. In all multipolar refinements, then, H atoms were kept fixed at positions resulting from model **2b**.

Differences between the high- and low-temperature geometries lie in the range of experimental standard deviations (*esd*) of the former model.[13] The disposition of ligands around Ni atom is pseudotetrahedral and the overall symmetry of the molecule has little distortion from 222 (D_2) symmetry. In fact, the root-mean-square deviation (RMSD) from the idealized D_2 symmetry molecule is 0.046 Å (if we consider only atoms involved in the π-bond systems, RMSD drops to 0.024 Å).

One of the main features observed is the elongation of C═C bonds (mean = 1.391(2) Å), which was originally considered as a proof of the DCD bonding scheme.[13] The other mean distances are Ni−C = 2.124(9) Å, $C(sp^2)-C(sp^3)$ = 1.519(2) Å, and $C(sp^3)-C(sp^3)$ = 1.543(4) Å. The pseudo 222 symmetry relates the C atoms, so that two classes of $C(sp^2)$, namely, C1 (C1A, C5A, C1B, C5B) and C2 (C2A, C6A, C2B, C6B), and two classes of $C(sp^3)$, C3 (C3A, C7A, C3B, C7B) and C4 (C4A, C8A, C4B, C8B), can be defined. The same partitioning can be done for H atoms too, so that six classes of hydrogens are recognized. For each C1−C2 pair, C2 is always closer to the metal than C1 (2.117(3) vs 2.130(9) Å), producing a distorted triangular ring in the Ni−L interaction. In Figure 1, the geometry of the $Ni(COD)_2$ molecule is shown.

It is worth noting the positive result of Hirshfeld rigid bond test[17] on atomic displacement parameters for all C−C bonds: the greatest difference between mean-squares amplitudes never exceeds 6×10^{-4} $Å^2$. In Ni−C bonds, instead, these differences are larger (≤ 1.6 10^{-3} $Å^2$) and they overcome the limit proposed by Hirshfeld (1.0×10^{-3} $Å^2$). However, a successful rigid-bond test should be expected only for a metallacycle system and, as we will see later, this is not the case; as a result Ni−C bonds have reduced covalent character and small bond orders. Moreover, Ni and C have significantly different atomic masses and this argument has been adopted for explaining similar "failures" of the Hirshfeld rigid bond test in other ED studies on transition metal complexes.[4f] The rigid bond test was also applied to all multipolar refinements performed and similar results were always obtained.

Multipolar Refinements and Determination of the Deformation Density. A multipole model was adopted to describe the deformation of $\rho(\mathbf{r})$ from spherical distribution. According to the method proposed

(8) According to Coppens, P. *Isr. J. Chem.* **1977**, *16*, 144−148 (a) and Feil, D. *ibid.* 149−153 (b) the ratio $s = V/\sum_j n_j^2$(core) (V is the cell volume and n is the number of core electrons for each j-th atom) is the best indicator for the suitability of ED studies (the higher the ratio, the better the system). Transition metal compounds always have very small values of S (<0.6), while for $Ni(COD)_2$ this ratio is considerably high, S = 0.83.

(9) The greatest difference in accuracy and overall costs between a conventional detector and a CCD area-detector collection is reached when dealing with *large* cell volumes, nevertheless the best absolute accuracy is still available when dealing with *small* volumes.

(10) The contamination of $\lambda/2$ has been demonstrated to be negligible for both crystal structure determination (Kirschbaum, K.; Martin, A.; Pinkerton, A. A. *J. Appl. Crystallogr.* **1997**, *30*, 514−516) and accurate charge density studies (ref 7b), thus a high voltage setting is not incorrect.

(11) This strategy provided 77% of data in $2\theta < 96°$(99% in $2\theta < 66°$).

(12) G. M. Sheldrick *SHELX-93: program for structure refinement*. University of Goettingen, Germany, 1994.

(13) Dierks, v. H.; Dietrich, H. *Z. Kristallogr.* **1965**, *122*, 1−23.

(14) Stewart, R. F.; Davidson, E. R.; Simpson, W. T. *J. Chem. Phys.* **1965**, *42*, 3175−3187.

(15) Stewart, R. F.; Bentley, J.; Goodman, B. *J. Chem. Phys.* **1975**, *63*, 3786−3793.

(16) Whenever a *mean* value is reported in the text or in the tables, the value in parentheses is the standard deviation of the average.

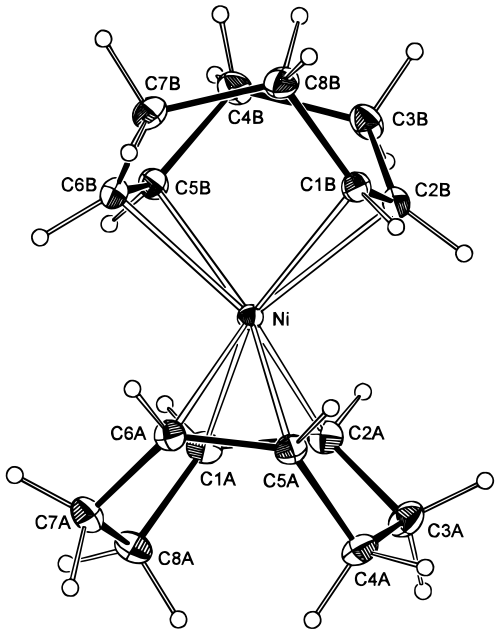

Figure 1. ORTEP view of Ni(COD)$_2$ molecule: thermal ellipsoid for non-H atoms are drawn at the 50% probability level (from model **2b**), while H atoms are idealized.

by Stewart,[18] the one electron density function $\rho(\mathbf{r})$ can be represented in terms of rigid pseudoatoms:

$$\rho(\mathbf{r}) = \sum_{i=1}^{N} \rho_i(\mathbf{r} - \mathbf{r}_i) \tag{1}$$

and each ρ_i in terms of multipoles,[19] with radial functions centered on nuclear positions:

$$\rho_i(\mathbf{r}_i) = P_{ic}\rho_{core}(\mathbf{r}_i) + P_{iv}\rho_{valence}(\kappa'\mathbf{r}_i) + \sum_{l=0}^{4}\left[R_l(\kappa''\mathbf{r}_i)\sum_{m=0}^{l} P_{ilm\pm} y_{lm\pm}(\mathbf{r}_i/r_i)\right] \tag{2}$$

where $y_{lm\pm}$ are spherical harmonics, $R_l(\mathbf{r})$ are the radial distribution functions, $P_{ilm\pm}$ are the population coefficients, and κ' and κ'' are the radial scaling parameters.

The choice of radial basis set and form factors is wide and sometime biases can be introduced in the model. Thus, to avoid a model-dependent interpretation of results, we performed several refinements using different "chemical" starting points (such as electronic configuration, distribution of charges, electroneutrality constraint, basis set for radial functions, etc.); moreover, the presence of a transition metal atom affords more uncertainty in its starting electronic configuration. Multipolar expansion was extended up to hexadecapole level for both Ni and C (when dealing with transition metal atoms expansion up to $l = 4$ is necessary[20]), and higher multipoles were introduced in a stepwise procedure;[21] H atoms were described with monopoles and dipoles.

The starting geometry was that obtained from refinement **2b** and reflections were considered up to $2\theta < 70°$ (*low order* refinement); only in the last steps the positional parameters for Ni and C were allowed to vary and all data available were used in the refinement.

Hartree−Fock (HF) atomic factors[22] were taken for core scattering (Ni and C) without refinement of core populations. Anomalous dispersion was included, while no extinction model was applied.

Valence monopole one-electron density functions for Ni ($4s^23d^8$) and C were taken equal to the HF expansions of Clementi and Roetti;[22] the 4s orbital population of Ni was kept fixed at 2.0. The radial part of higher multipoles of Ni were constructed by using HF 3d orbitals, while single ζ Slater functions were used for C ($\zeta(C) = 3.44$ bohr^{-1}; $n_l = 2, 2, 3, 4$ for dipole, quadrupole, octupole, and hexadecapole, respectively[23]). Hydrogen monopole and dipoles were single ζ Slater functions ($\zeta(H) = 2.48$ bohr^{-1}; $n_l = 0, 1$). Two parameters (κ'_{Ni} and κ'_C) scaling spherical radial density of Ni and C were refined; κ''_{Ni}, scaling the radial deformation functions of Ni, was constrained equal to κ'_{Ni} to avoid divergence; κ''_C scaling ζ(C) was also refined, while ζ(H) was kept fixed (model **3a**).

Significantly worse agreement indexes were found upon introduction of different electronic configurations for Ni (such as $4s^13d^9$ and $3d^{10}$);[24] physically meaningless coefficients were obtained when a 4s population refinement was separately tried. Refinement of κ'_H scaling ζ(H) was not possible, since some unrealistic isotropic thermal factors for hydrogen atoms were obtained. We also tried to use Slater-type functions for the radial distribution of Ni multipoles, but no improvement was gained, while a more difficult interpretation of topological analysis resulted.

Due to the pseudo 222 arrangement of ligand atoms around the metal, multipole coefficients of *pseudoequivalent* atoms closely resemble each other (once the proper local reference systems have been defined). This suggests that one can constrain their electronic populations as we initially did within C1 and C2 classes only; moreover, monopoles of chemically equivalent hydrogens (H vinylic and H methylenic) were imposed to be equal; the number of parameters dropped from 702 to 530 (model **3b**). The extension of the D_2 population symmetry also to C3 and C4 resulted in a worse fitting, as expected from the larger (geometrical) deviation of the "external" atoms from the idealized D_2 symmetry. Worse fitting also resulted by imposing a D_2 symmetry restraint to Ni multipoles. This may be related either to a larger sensibility of Ni to the lack of *true* 2-fold axes or to the difficulty of defining its local coordinate system,[25] indeed, in refinements **3a** and **3b** (with unconstrained Ni populations) some of the multipole terms *not-allowed* by D_2 site-symmetry had nonnegligible values (see Table 3).

Finally, we have carefully compared models **3a** and **3b**: the latter had slightly worse agreement indexes; the rigid bond test was successful for C−C bonds (the maximum difference between mean-squares amplitudes was 7×10^{-4} for **3a** and 4×10^{-4} for **3b**), but still failed for Ni−C bonds; uncertainties in multipolar and thermal parameters were reduced in **3b**, while atomic positions had larger *esd*'s; correlation coefficients were drastically reduced in the *chemically constrained* model (in particular monopoles and isotropic thermal factors for hydrogens); QTAM analysis also indicated **3b** as the most satisfactory model (see footnote of Table 4).

Agreement indexes and final values of κ_i' and κ_i'' for **3a** and **3b** are reported in Table 2. Atomic positions, thermal parameters, and multipolar coefficients (model **3b**) are included as Supporting Information.

Computational Details. All multipolar refinements were carried by using the XD software package:[26] the quantity minimized was $\epsilon = \sum w(F_o^2 - F_c^2)^2$ based on the 9369 reflections with $I > 0$; weights were

(17) Hirshfeld, F. *Acta Crystallogr.* **1976**, *A32*, 239−244.

(18) Stewart, R. F. *Acta Crystallogr.* **1976**, *A32*, 565−574.

(19) Hansen, H. K.; Coppens, P. *Acta Crystallogr.* **1978**, *A34*, 909−921.

(20) (a) Holladay, A.; Leung, P.; Coppens, P. *Acta Crystallogr.* **1983**, *A39*, 377−387. (b) Stevens, E. D.; Coppens, P. *Acta Crystallogr.* **1979**, *A35*, 536−539. (c) Stewart, R. F. *J. Chem. Phys.* **1973**, *58*, 1668−1676.

(21) We applied the statistical test reported in: Prince, E.; Spiegelman, C. H. In *International Tables for Crystallography* Wilson, A J. C., Ed.; Kluwer Academic Publishers: Dordrecht, 1995; Vol. C, pp 618−624. (This has been already employed for comparing different refinements in electron density determinations; see ref 2d. We use it to verify that the expansion of the set of parameters by including a higher multipole gave significant improvement to the fit.

(22) Clementi, E.; Roetti, C. *At. Data Nucl. Data Tables* **1974**, *14*, 177−478.

(23) Hehre, W. J.; Stewart, R. F.; Pople, J. A. *J. Chem. Phys.* **1969**, *51*, 2657−2664.

(24) In references 4f and 4g the authors demonstrated the important contribution of expanded 4s orbitals and that taking into account contracted 3d orbitals only produces a significant loss in model flexibility.

(25) We have used a coordinate system defined by the three (orthogonal) 2-fold axes in the symmetrized molecule.

(26) Koritsanszky, T.; Howard, S. T.; Su, Z.; Mallinson, P. R.; Richter, T.; Hansen, N. K. *XD, Computer Program Package for Multipole refinement and Analysis of Electron Densities from Diffraction Data*, Free University of Berlin, Germany, June, 1997.

Table 2. Results of Multipolar Refinement[a]

	model				
	1	**2a**	**2b**	**3a**	**3b**
reflectns	9369	9369	9369	9369	9369
params	250	250	250	702	530
R_1 (%)	2.16	2.23	2.20	1.64	1.68
wR_1 (%)		1.95	1.99	1.13	1.19
R_2 (%)		3.19	3.20	2.01	2.13
wR_2 (%)	4.43	3.86	3.94	2.23	2.36
GoF	0.929	1.46	1.47	0.87	0.91
κ'_{Ni}				0.975(3)	0.964(3)
κ'_{C}				0.960(3)	0.954(4)
κ''_{C}				0.824(6)	0.831(6)
scale factor	0.5436(2)	0.5434(2)	0.5432(2)	0.5465(9)	0.5491(9)

[a] Models are fully described in the text. $R_{int} = \sum|F_o^2 - F_{mean}^2|/\sum F_o^2$; $R_\sigma = \sum\sigma(F_o^2)/\sum F_o^2$ $R_1 = \sum||F_o| - |F_c||/\sum|F_o|$; $wR_1 = (\sum(F_o - F_c)^2/\sum wF_o^2)^{1/2}$; $R_2 = \sum||F_o^2| - |F_c^2||/\sum|F_o^2|$; $wR_2 = (\sum(F_o^2 - F_c^2)^2/\sum wF_o^4)^{1/2}$.

Table 3. Multipole Populations of Atoms Ni, C1, and C2 (model **3b**)[a]

$P_{lm\pm}$	Ni	C1	C2	$P_{lm\pm}$	Ni	C1	C2
P_{00}	7.91(3)	4.25(3)	4.26(3)	P_{32-}	0.009(8)	0.0269(9)	−0.014(9)
P_{11+}	−0.01(1)	−0.03(1)	0.05(1)	P_{33+}	−0.005(8)	−0.032(9)	0.04(1)
P_{11-}	0.02(1)	0.03(1)	0.04(1)	P_{33-}	0.004(8)	−0.24(1)	−0.26(1)
P_{10}	−0.02(1)	−0.02(1)	−0.003(9)	P_{40}	0.14(1)	0.044(9)	−0.00(1)
P_{20}	−0.07(1)	−0.097(8)	−0.090(8)	P_{41+}	0.06(1)	0.009(8)	−0.007(9)
P_{21+}	0.11(1)	0.032(7)	−0.030(8)	P_{41-}	−0.02(1)	−0.06(1)	−0.07(1)
P_{21-}	−0.02(1)	0.082(9)	0.121(9)	P_{42+}	0.02(1)	0.00(1)	−0.01(1)
P_{22+}	0.11(1)	−0.003(9)	0.00(1)	P_{42-}	−0.03(1)	0.01(1)	0.00(1)
P_{22-}	−0.14(1)	0.032(9)	−0.026(9)	P_{43+}	−0.05(1)	−0.00(1)	−0.02(1)
P_{30}	0.0010(8)	0.136(9)	0.144(9)	P_{43-}	0.008(11)	0.05(1)	0.04(1)
P_{31+}	0.026(8)	0.017(7)	0.004(8)	P_{44+}	−0.05(1)	−0.01(1)	0.02(1)
P_{31-}	0.003(8)	−0.058(8)	−0.029(8)	P_{44-}	−0.28(1)	0.01(1)	−0.00(1)
P_{32+}	0.017(8)	−0.151(9)	−0.16(1)				

[a] Local coordinate systems: Ni (*x*, *y*, and *z* oriented as the *pseudo-2-fold* axes, see **III**); C1 (*z* C1−Ni, *y* C1−C2); C2 (*z* C2−Ni, *y* C2−C1).

Table 4. Results of the Topological Analysis of $\rho(\mathbf{r})$ for All Bonds[a]

atom1−atom2	model	*d*	*r*1	*r*2	$\rho(\mathbf{r}_b)$	$\nabla^2\rho(\mathbf{r}_b)$	λ_1	λ_2	λ_3	*n*(exp)	*n*(EHT)	ϵ
Ni−C1		2.130(9)									0.33	
	3a		1.056(3)	1.081(8)	0.547(3)	4.79(2)	−2.43(5)	−0.80(11)	8.0(2)	0.346(1)		2.0(3)
	3b		1.056(3)	1.083(8)	0.548(7)	4.98(4)	−2.36(5)	−0.69(8)	8.03(15)	0.344(2)		2.5(3)
Ni−C2		2.117(3)									0.31	
	3a		1.055(2)	1.065(2)	0.542(8)	4.75(6)	−2.50(3)	−0.93(4)	8.18(5)	0.345(3)		1.70(12)
	3b		1.057(2)	1.079(2)	0.543(4)	5.39(7)	−2.30(3)	−0.39(7)	8.08(5)	0.342(1)		5.1(1.3)
C1−C2		1.391(2)									1.51	
	3a		0.684(1)	0.709(1)	2.177(6)	−21.92(14)	−15.50(5)	−13.68(4)	7.26(5)	1.768(10)		0.130(1)
	3b		0.691(2)	0.702(1)	2.137(7)	−20.83(13)	−15.11(4)	−12.79(4)	7.07(5)	1.685(12)		0.180(1)
C1−C4; C2−C3		1.519(3)									1.01	
	3a		0.781(1)	0.738(2)	1.70(6)	−13.2(8)	−11.3(5)	−10.7(5)	8.7(2)	1.10(7)		0.056(5)
	3b		0.773(9)	0.746(7)	1.67(4)	−13.2(1.2)	−11.2(4)	−10.4(7)	8.3(3)	1.06(4)		0.08(6)
C3−C4		1.543(4)									0.98	
	3a		0.783(2)	0.760(2)	1.608(8)	−11.4(2)	−10.41(8)	−9.89(6)	8.86(3)	1.000(8)		0.053(5)
	3b		0.782(14)	0.762(11)	1.61(2)	−12.3(8)	−10.8(4)	−10.0(4)	8.5(2)	1.00(2)		0.08(2)
C1−H; C2−H		1.08(2)									0.97	
	3a		0.702(12)	0.382(11)	1.71(8)	−15(2)	−15.4(1.1)	−14.8(1.2)	14.9(6)	1.12(9)		0.044(7)
	3b		0.717(12)	0.367(7)	1.76(3)	−16.7(6)	−16.3(4)	−15.7(3)	15.4(4)	1.16(3)		0.041(8)
C3−H; C4−H		1.09(2)									0.97	
	3a		0.679(13)	0.415(11)	1.77(8)	−15(2)	−15.2(8)	−14.3(1.0)	14.5(6)	1.18(9)		0.07(2)
	3b		0.682(14)	0.412(13)	1.76(5)	−15(2)	−15.4(7)	−14.2(8)	14.3(9)	1.16(5)		0.09(3)

[a] Refinement **3a** afforded an unreasonable, asymmetric disposition of bcp's for Ni(C1 = C2) bonds, unless the topological properties of *pseudoequivalent* bonds were averaged. Accordingly, to obtain averaged values close to those from "raw" populations (not tabulated here) but with a smaller spread of "equivalent" properties, the population parameters of *pseudoequivalent* atoms were merged before applying the topological search of cp's (rows **3a**). However, the best way to deal with this problem was to resort to the *chemically constrained* model **3b**, whose topological results are quite similar (rows **3b**). *d* is the interatomic distance (Å); *r*1 and *r*2 are the distances (Å) of atom 1 and 2 from bcp; $\rho(\mathbf{r_b})$ (e Å^{-3}), $\nabla^2\rho(\mathbf{r_b})$ (e Å^{-5}), and λ_i's (e Å^{-5}) are properties calculated at bcp's. *n*(exp) is the experimental bond order; *n*(EHT) is the Mayer bond index, calculated within EHT; ϵ is the bond ellipticity. Values in parentheses are the estimated standard deviations from the average.

always taken as $w = 1/\sigma^2(F^2)$. Convergence was assumed when $|\delta(\epsilon)/\epsilon| = (\epsilon_n - \epsilon_{n-1})/\epsilon| \leq 10^{-5}$ (where n is the number of cycles).

As for topological analysis, critical points of the electron density were searched via a Newton Raphson algorithm implemented in XD. Properties of $\rho(\mathbf{r})$ and $\nabla^2\rho(\mathbf{r})$ were calculated after transformation of the local axis system into a global system and in each point contributions from atoms located in a sphere of radius 6.0 Å were considered.

Hirshfeld charges were computed integrating the defined function[27] over all space with a Gaussian 3D quadrature algorithm, locally implemented in XD.

Extended Hückel calculations were performed on the symmetrized molecule with a local version of CACAO[28] (modified to compute Mayer

(27) Hirshfeld, F. L. *Theor. Chim. Acta* **1977**, *44*, 129−138.

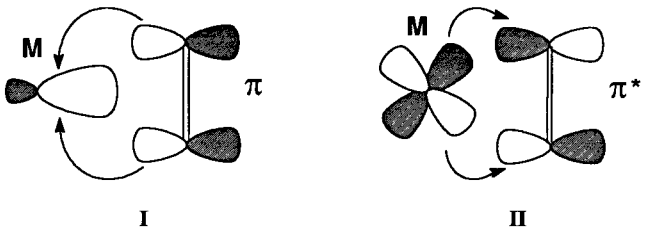

I II

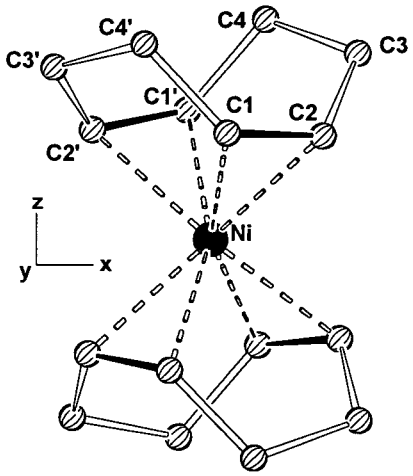

III

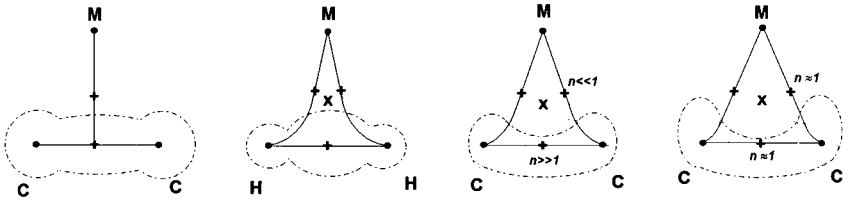

A B C D

bond indexes), using recently tabulated parameters for transition metal atoms.[29]

Results and Discussion

The bonding between a transition metal atom and a π-ligand is easily explained by the classical Dewar Chatt Duncanson (DCD) model.[6] Two different effects are involved: an electron density flow from the filled π orbital of the ligand into suitably directed metal orbitals (σ donation, **I**) and a reverse flow from filled metal d orbitals into ligand empty π^* orbital (π back-donation, **II**).

We have performed EHT calculations on a symmetry idealized $Ni(COD)_2$ molecule in order to clarify some stereochemical aspects regarding the experimental d-orbital occupancies to depict a starting orbital picture of the bonding and to test the internal coherence of experimental bond orders (vide infra) by computing Mayer's bond indexes.[30] These calculations suggest that Ni cannot accept ligand electrons to a great extent (**I**) and that π back-donation (**II**), which mainly involves d(xz) and d(yz) orbitals and marginally d(x^2-y^2), is slightly hampered by the *pseudotetrahedral* arrangement of ligands. This agrees with the small Ni−C bond orders and the $Ni(COD)_2$ lability. As a matter of fact, at room temperature the complex is oxidized in air and easily undergoes ligand substitution (it is commonly used in organometallic chemistry as a starting reagent).

The reference system and the labels for the idealized D_2 structure of the molecule are reported in **III** and are fully coherent with those used in multipolar refinements, topological analysis and d electron partitioning.

Previous theoretical work on $Ni(C_2H_4)_n$ ($n = 1-4$)[31] demonstrated that the DCD approach is substantially correct and that back-donation is comparable in strength to donation itself. DCD model allows an explanation of a number of experimental observations—ranging from the lengthening of intraligand double bonds to the actual orientation of π-ligands with respect to the remaining fragment—but, it is not suited to quantify the different bonding properties of different ligands. In other words, while for most organic systems theoretical chemistry well supports a simple (Lewis) formalism for drawing (defining) bonds, in π-complexes such a scheme does not emerge in a straightforward manner. In fact, we cannot state whether the two C atoms are *independently* bounded to the metal or if an overall three center interaction is a better representation, nor can we distinguish a π-bonded complex from a metallacycle. Possibly, the fact that ligand donation concentrates electrons in the inner region of the MC_2 triangle while back-donation spreads them about the two M−C edges will allow a clearer picture to emerge upon the topological analysis of the electron density, which we address experimentally in this paper.

(28) Mealli, C.; Proserpio, D. M. *J. Chem. Educ.* **1990**, *67*, 399−402.
(29) Macchi, P.; Proserpio, D. M.; Sironi, A. *Organometallics* **1997**, *16*, 2101−2109.
(30) Mayer, I. *Chem. Phys. Lett.* **1983**, *97*, 270−274.
(31) (a) Siegbahn, P. E. M.; Brandemark, U. B. *Theor. Chim. Acta* **1986**, *69*, 119−133. (b) Widmark, P. O.; Roos, B. O.; Siegbahn, P. E. M. *J. Phys. Chem.* **1985**, *89*, 2180−2186. (c) Rösch, N.; Hoffmann, R. *Inorg. Chem.* **1974**, *13*, 2656−2666.

Topological Analysis. The distribution of electron density can be studied within the well-known approach of *atoms in molecules* and the topological analysis of $\rho(\mathbf{r})$.[1] Although it was introduced and first applied only to theoretical electron density, topological analysis has been, later, applied to experimental $\rho(\mathbf{r})$ as well, and up to now several studies proving its general validity are known.[32]

Bader's analysis directly deals with $\rho(\mathbf{r})$; atoms and bonds can be clearly related to properties of the density distribution. Points where the gradient of total electron density, $\nabla\rho(\mathbf{r})$, vanishes are called *critical points* (cp) and they can be classified on the basis of rank and signature of the Hessian matrix as determined by its eigenvalues λ_i ($i = 1-3$). Thus (3,−3) cp's (*rank* = +3; *signature* = −3) are maxima of $\rho(\mathbf{r})$ and they correspond to nuclear positions; (3,−1) cp's are called *bond critical points* (bcp, $\mathbf{r_b}$) because they are found between two bounded atoms connected by a path of maximum electron density (med) called *bond path* (the two curvatures perpendicular to the bond path are negative, while the other along the med is positive). (3,+1) cp's are called *ring critical points* (rcp, $\mathbf{r_r}$) always found in the middle of a cyclic structure, the negative curvature being directed outside the plane of the ring; finally, (3,+3) cp's are called *cage critical points* (ccp).

Properties of $\rho(\mathbf{r})$ at cp's are related to the nature of the chemical bond:[1b] *ellipticity* (ϵ[33]) affords information about the anisotropic distribution of the density along the bond; the *Laplacian* $[\nabla^2\rho(\mathbf{r})]$ allows one to distinguish between covalent open-shell $[\nabla^2\rho(\mathbf{r_b}) < 0]$ or closed-shell $[\nabla^2\rho(\mathbf{r_b}) > 0]$ interactions; the *bond paths* (bp) reveal the bent-bond character. We have also computed other useful indicators for a complete bond analysis.

(1) Bond Order (*n*): The value of $\rho(\mathbf{r_b})$ has been related to the order of the chemical bond by a simple exponential formula:[1b]

$$n = \exp\{A[\rho(r_b) - B]\} \tag{3}$$

where A and B are parameters that are usually determined by fitting $n = 1$ and $n = 2$ using $\rho(\mathbf{r_b})$ of ethane and ethylene C−C bonds. A and B strongly depend on the basis set used for computing $\rho(\mathbf{r})_{\text{theor}}$, thus in the literature different values for A and B are reported. Here, we deal with an *experimental* $\rho(\mathbf{r})$ and no comparison with bonds of *reference* molecules is, actually, possible. Moreover, we cannot fit two reference bonds (single and double) within the title molecule, because all the double bonds in $Ni(COD)_2$ are themselves the matter of our study. Thus, considering that A has generally a value very close to 1.0, we kept this parameter fixed at 1.0 and fitted B with the averaged $\rho(\mathbf{r_b})$ for Csp^3-Csp^3 (C3−C4) single bond.

(2) Nonpolar Midpoint: The distance of $\mathbf{r_b}$ from the geometrical midpoint of the internuclear vector is a measure of the polarity of the bond (bcp's are always shifted toward the less electronegative atom). It has also been proposed[34] to consider the shift from a *weighted* nonpolar midpoint (m). For a A_1-A_2 bond we can evaluate

$$m_1 = r_1 r_{12}(r_1 + r_2)^{-1} \tag{4}$$

m_1 is the distance of the nonpolar midpoint from atom A_1, r_1 and r_2 are the covalent radii of A_1 and A_2, respectively, and r_{12} is A_1-A_2 bond distance (of course $m_2 = r_{12} - m_1$).

Three membered rings of main group atoms have been carefully studied within QTAM by using theoretical approaches;[35] in particular comparisons of cyclopropane with other substituted analogues supported the bent bond theory when the covalent character dominates, while T-shaped structures were found when the interaction is mainly ionic. Few examples of $X_nM-(\eta^2\text{-ligand})$ bond treated with a topological analysis of the (theoretical) $\rho(\mathbf{r})$ are, instead, known in the literature; basically we may recognize four different models:

(**a**) Ionic, e.g., $[Cu(C_2H_4)]^+$:[36] No rcp is there; the bcp of C−C bond and only one bcp between M and the ligand are found; the bond path can be drawn as a straight line from the metal to the center of the C═C bond (T-shaped bonding, see **A**, where solid lines represent bp). The Laplacian around the ligand is only slightly distorted from that of a free ethylene (dashed line in **A**−**D** represents the zero level contour of $\nabla^2\rho(\mathbf{r})$, and its envelope contains the region of negative Laplacian[37]).

(**b**) σ-Donation of a σ-bond *plus* back-donation into a σ^*-orbital, e.g. $(CO)_5W(H_2)$:[38] a ring structure (concave shape) is recognized with one H−H and two M−H bcp's and a central rcp; the bp is strongly curved *inwardly* (**B**) and the Laplacian indicates a charge concentration in the center of H−H bond toward the metal.

(**c**) σ-Donation of a π-bond *plus* back-donation into a π^*-orbital (DCD model, *e.g.* $(CO)_5W(C_2H_4)$):[39] A ring structure is found; the bond path between M and C is less curved *inwardly* and resembles a straight line except in the proximity of C atoms, where it holds a concavity; the Laplacian shows two charge concentrations in correspondence of carbon π-orbitals (see **C**). On increase in the amount of back-donation and covalency of the M−C interactions the C−M−C bp angle widens, leading to bp and $\nabla^2\rho(\mathbf{r})$ similar to those in **D**. The bond orders of M−C and C−C bonds are quite different: $n_{C-C} \gg n_{M-C}$ (ca. 1.6 vs 0.4).

(**d**) Metallacycle (e.g., $Cl_4W(C_2H_4)$):[39] Although the topology is substantially similar to that in **C**, charge concentration along the M−C bonds is more pronounced and the concavity of bp at C is reduced (see **D**); the DCD model does not work anymore and only the presence of two M−C covalent interactions can actually account for the bonding; moreover, $n_{C-C} \approx n_{M-C}$ (ca. 1.1 vs 0.9).[39b]

Summarizing, *pure* closed shell interactions lead to T-shape structures (**A**), otherwise *concave* cycles are present (**B**-**D**); the increase of π-back-donation and hybridization on ligand atoms widens all bond path angles (up to **D**), eventually leading to a true metallacycle (**d**). Moreover, judging from the shape of $\nabla^2\rho(\mathbf{r})$ zero level, the covalent character of the M−C interactions increases from **a** to **d** as a consequence of the decreased difference in electronegativity ($\Delta\chi$) between the MX_n and the ligand fragments; eventually if $\Delta\chi = 0$ (i.e., CH_2 replaces MX_n), the *convex* ring structure of cyclopropane arises (Figure 2a). Note that, from a chemical point of view, the topological definition of a cyclic structure does not necessarily require a

(32) See, for example: Gatti, C.; Bianchi, R.; Destro, R.; Merati, F. *J. Mol. Struct. (Teochem)* **1992**, *255*, 409−433.

(33) $\epsilon = \lambda_1/\lambda_2 - 1$, where λ_1 and λ_2 are the two negative eigenvalues ($|\lambda_1| > |\lambda_2|$) and their eigenvectors are perpendicular to the bond path.

(34) Otto, M.; Lotz, S. D.; Frenking, G. *Inorg. Chem.* **1992**, *31*, 3647−3655.

(35) Cremer, D.; Kraka, E. *J. Am. Chem. Soc.* **1985**, *107*, 3800−3810.

(36) Böhme, M.; Wagener, T.; Frenking, G. *J. Organomet. Chem.* **1996**, *520*, 31−43.

(37) Of course, the atomic electronic structure is not considered in this context.

(38) Dapprich, S.; Frenking, G. *Angew. Chem.* **1995**, *107*, 383; *Angew. Chem., Int. Ed. Engl.* **1995**, *34*, 354−357.

(39) (a) Pidun, U.; Frenking, G. *Organometallics* **1995**, *14*, 5325−5336. (b) Frenking, G.; Pidun, U. *J. Chem. Soc., Dalton Trans.* **1997**, 1653−1662. (c) For alkyne complexes, see: Stegmann, R.; Neuhaus, A.; Frenking, G. *J. Am. Chem. Soc.* **1993**, *115*, 11930−11938.

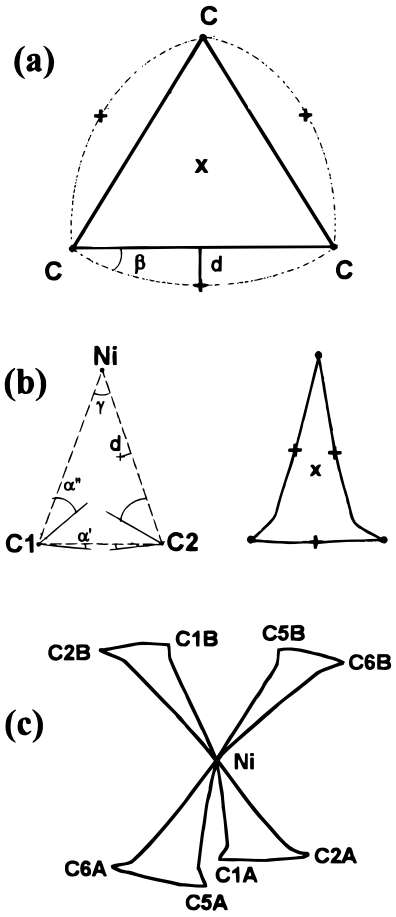

Figure 2. (a) A schematic bond path draw of cyclopropane, idealized from theoretical results:[35] $\beta(=9.42°)$, $d = 0.06$ Å; the bond path length is 1.507 Å, while the C−C distance is 1.497 Å. (b) Bond path in Ni−(C1=C2) ring, from model **3b**: the geometrical ring (left) is compared to the bond path ring obtained upon topological analysis of experimental $\rho(\mathbf{r})$ (right). α′ is the takeoff angle between C−C bond path and the internuclear vector: α′(C1) = 5.42(7)°; α′(C2) = 2.91(5)°. α″ is the angle in C−Ni direction: α″(C1) = 25(2)°; α″(C2) = 36(2)°. The bond path angle at Ni, $\gamma = 24(2)°$is less than the geometrical one (=38.1(1)°). The averaged bp lengths are: Ni−C1 = 2.167(14) Å; Ni−C2 = 2.194(6) Å; C1−C2 = 1.398(2) Å, while the geometric vectors are 2.130(9), 2.117(3), and 1.391(2) Å, respectively. The distances between each bcp and the geometric bond (d in figure) are 0.101(8) and 0.144(10) Åinside the ring for Ni−C1 and Ni−C2 and 0.032(1) Å outside the ring for C1−C2. (c) The complete bond path for the π-system. Note the eight med lines that link Ni to each C(sp^2) atom.

metallacycle; in fact a metallacycle is predicted only for **d** while a cyclic topological structure is also seen in **b** and **c**.[40]

All multipolar models for Ni(COD)$_2$, upon application of topological analysis, share some common features, which may be resumed in the following.

(1) Ni−C bonds (Ni−C1 and Ni−C2): We identified 8 med lines and related bcp's, linking Ni with each C(sp^2) atom; each bond path is nearly a straight line with a concavity at C atoms and it lies inside the three membered ring (Ni, C1, C2, see **III** and Figure 2b); the C1−Ni−C2 bond path angle is less than the geometrical one; the angle between the internuclear vector C−M and the bond path at C (α″(C) in Figure 2b) is quite large. $\nabla^2\rho(\mathbf{r_b})$ is positive but less than that expected for similar closed shell interactions.[41] The values of $\rho(\mathbf{r_b})$ indicates a low bond order, in good agreement with Mayer bond indexes calculated within the EHT method (see Table 4), with the large bond path lengths ($bp_{Ni-C} \gg d_{Ni-C}$) and with the small Ni−C−C bond path angles (see Figure 2). Although $d_{Ni-C1} > d_{Ni-C2}$, n_{Ni-C1} is greater than n_{Ni-C2}, and this might be due to a slightly different hybridization of the two carbons as also evidenced by bond path lengths ($bp_{Ni-C2} > bp_{Ni-C1}$) and takeoff angles (α″(C2) > α″(C1)). Note that a similar dependence of $\rho(\mathbf{r_b})$ on the bp length rather than on the actual atomic distance was also found in compound of ref 4f, in which d_{Ni-N} and d_{Ni-O} are similar, but $bp_{Ni-N} \ll bp_{Ni-O}$, thus $\rho(\mathbf{r_b})_{Ni-N} \gg \rho(\mathbf{r_b})_{Ni-O}$.

Table 5. Averaged Results of a Ring Critical Point Search in the Three and Five Membered Rings (Model **3b**) (Units as in Table 4)

	three membered ring	five membered ring
d(Ni−$\mathbf{r_r}$)	1.063(2)	1.571(12)
d(C1−$\mathbf{r_r}$)	1.204(12)	1.43(2)
d(C2−$\mathbf{r_r}$)	1.144(13)	1.434(13)
d(C3−$\mathbf{r_r}$)		1.508(7)
d(C4−$\mathbf{r_r}$)		1.55(2)
$\rho(\mathbf{r_r})$	0.541(5)	0.19(4)
$\nabla^2\rho(\mathbf{r_r})$	5.55(6)	2.00(14)
λ_1	−2.28(3)	−0.47(12)
λ_2	0.28(3)	0.95(11)
λ_3	7.55(12)	1.5(2)

The average ellipticity is very high with charge concentrated in the plane of the ring. As for the polarity, the bcp is slightly shifted toward Ni, considering either the *geometrical* or the *nonpolar* midpoints.[42]

(2) Three membered rings (Ni, C1, C2): A rcp has been located in the center of each of the four rings; $\nabla^2\rho(\mathbf{r_r})$ is positive; $\rho(\mathbf{r_r})$ is very similar to the two corresponding $\rho(\mathbf{r_b})$'s ($\Delta[\rho(\mathbf{r_b}) - \rho(\mathbf{r_r})] \cong 0.01-0.03$ eÅ^{-3}, while in cyclopropane this difference is 0.30 eÅ^{-3}), i.e., the curvature of $\rho(\mathbf{r})$ is very low inside the cycle, mainly because of the small C1−Ni−C2 angle, which shortens the $\mathbf{r_r}-\mathbf{r_b}$ distances. Like $\mathbf{r_b}$, $\mathbf{r_r}$ also is closer to Ni than to C atoms (see Table 5). We want to remark that without the refinement of κ parameters and hexadecapole populations on C atoms, it was not possible to determine the ring structure topology, because the rcp and the two bcp's all collapse into one single bcp for each triangular ring (nearly in the same position of the rcp), thus suggesting a T-shaped binding.[43] Probably, the very low curvature of $\rho(\mathbf{r})$ inside the ring and the relative closeness of the critical points ($d_{bcp-rcp} <$ 0.30 Å) do require the *greatest* deformation description on all pseudoatoms to make the ring structure recognized. Moreover, a description of C atoms expanded up to hexadecapole level was statistically superior to that with carbons truncated at octopoles.[21]

(40) Strictly speaking, a "true metallacycle" should have n(M−C) = n(C−C) = 1.0, *not-interrupted* region of negative Laplacian along M−C bonds and *not-inwardly* curved bond paths. However, $X_nM(\eta^2$-L) can hardly reach this limit (at least no example is known). We are then well aware that, although the two extreme bond types are well characterized and distinguishable, a boundary cannot be defined. However, all examples reported in ref 39 stay far apart from the *borderline* zone and they can be undoubtedly classified into **c** or **d**. On the basis of the bond order, also for Ni(COD)$_2$ no ambiguity arises (vide infra).

(41) For instance, in ref 4a of $\nabla^2\rho(\mathbf{r_b}) = 12.1$ e Å^{-5} for Co−N interactions; in ref 4f $\nabla^2\rho(\mathbf{r_b}) = 9.8$ e Å^{-5} for Ni−O bonds, and in ref 4g $\nabla^2\rho(\mathbf{r_b}) = 7.1$ and 9.9 e Å^{-5} for two kinds of Ni−N bonds. However, in 4f the Ni−N interaction has a larger amount of covalency, in fact $\nabla^2\rho(\mathbf{r_b}) =$ 1.4 e Å^{-5}.

(42) Kilbourn, B. T.; Powell, H. M. *J. Chem. Soc.* **1970**, *A*, 1688−1693. In this ref the estimated covalent radii of Ni in tetrahedral complexes is 1.21 Å, thus for Ni−C1 $m_{Ni} = 1.30$ Å, for Ni−C2 $m_{Ni} = 1.29$ Å.

(43) Actually, a more careful analysis of $\nabla\rho(\mathbf{r})$ made us able to find out the three different *cp*'s, all positioned very close to each other in the center of the ring, but their attribution, based on the signature of the Hessian matrix, was not undoubted (being one value of λ_i less than its *esd*).

(3) $C(sp^2)-C(sp^2)$ bonds (C1−C2): $\rho(\mathbf{r_b})$ is smaller than that of other double bonds (2.15 vs 2.2−2.45 e Å^{-3}),[44] as a consequence, the normalized bond order is reduced, in agreement with EHT prediction. The ellipticity is also smaller (0.18 vs 0.45−0.82) and its decrease is due to σ-donation only (the π back-donation being ineffective on ϵ). It is noteworthy that the topological interaction between bcp's and rcp's which causes the reduced ϵ of cyclopropene with respect to cyclobutene[44] should, instead, enhance ϵ in $Ni(COD)_2$ (the major axis of π-density lying in the ring rather than being perpendicular to it).[45] The bond path is not a straight line, but it is slightly curved outside the ring formed with Ni, thus its length is increased (see Figure 2b). The Laplacian distribution differs from that of normal double bonds mainly because of the presence of regions of charge concentration along the two C−Ni bonds (see Figure 3a).

(4) $C(sp^2)-C(sp^3)$ and $C(sp^3)-C(sp^3)$ bonds: They all show little ellipticity, probably due to the conjugation with π bonds. Averaged bond orders for $C(sp^2)-C(sp^3)$ are more than 1.0 (see Table 4).

(5) C−H bonds: All expected bcp's are found. The bond order is greater than 1.0, probably because a radial scaling of H monopoles was not refinable.

(6) Five membered rings (Ni, C1,C4′,C3′, and C2′ in **III**): Rcp's are found in each of these four cycles; the distance from the least-squares plane defined by the five atoms is about 0.1 Å; $\rho(\mathbf{r_r})$'s are very small, because these rings are quite large (see Table 5).

(7) No ccp was found, nor was any other *intramolecular* critical point; note that the presence of four additional rcp's (point **6**) and the simultaneous absence of ccp's are required by the Poincaré-Hopf rule for an isolated molecule:[46]

$$c - r + n - N = -1 \qquad (5)$$

where c is the number of ccp's, r the number of rcp's, N the number of nuclei, and n the number of bcp's. Here, $c = 0$, $r = 8$, $n = 48$, and $N = 41$.[47]

(8) Although our study is strongly concerned with the application of Bader's theory to experimental $\rho(\mathbf{r})$, we have also computed the static deformation density, $\Delta\rho(\mathbf{r})$, which is totally coherent with the above topological description. In fact, two M−C distinct bonding regions are found and the distribution around the C−C double bond is clearly distorted toward the metal (see Figure 3b).

Topological properties and the Laplacian distribution around the ligand speak for a donor−acceptor complex, suggesting a behavior very similar to that previously depicted in point **c**. Features of $\nabla^2\rho(\mathbf{r})$ along M−C bonds and its values at *cp*'s indicate a certain degree of covalency for the M−L interactions, which are, however, rather weak, according to the normalized bond orders and the bond path lengths. Moreover, the results of Hirshfeld's rigid bond test along the Ni−C directions suggest the softness of such stretching modes and, perhaps, the weakness of the metallacycle hypothesis. Visually judging, the deformations of the Laplacian reported in refs 39a,b for $(CO)_5W(C_2H_4)$ are somewhat smaller than those in $Ni(COD)_2$ (Figure 3a). This fact, which is in agreement with the larger electronegativity of Ni as respect to W,[29] suggests that the title compound is

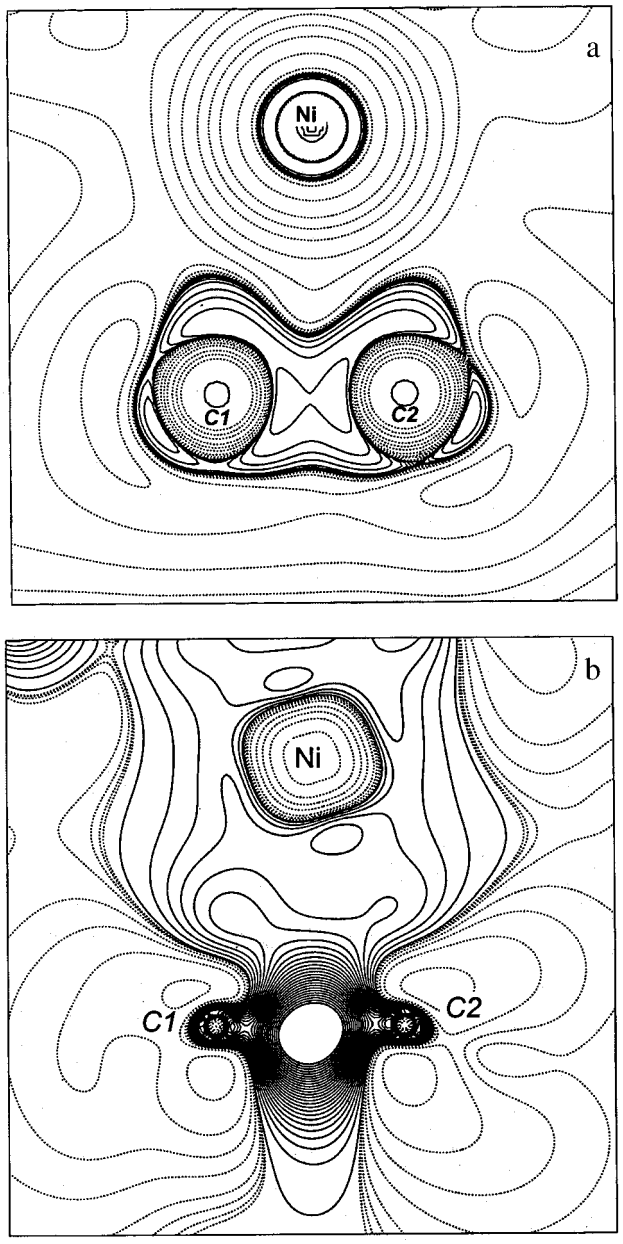

Figure 3. (a) A plot of Laplacian distribution in the plane defined by Ni C1 and C2. Dot contours refer to positive values of $\nabla^2\rho(\mathbf{r})$, solid lines to negative Laplacian. Contours are drawn at $\pm2.0 \times 0^x$, $\pm4.0 \times 10^x$, $\pm8.0 \times 10^x$ e Å^{-5} levels ($x = -2, -1, 0, +1$). Notice the significant distortion toward the metal atom. (b) As a comparison we report also the distribution of the static $\Delta\rho(\mathbf{r})$ in the same plane; dot lines are negative contours. Note the distortion toward Ni and the two distinct M−L bond regions.

(44) Bader, R. F. W.; Slee, T. S.; Cremer, D.; Kraka, E. *J. Am. Chem. Soc.* **1983**, *105*, 5061−5068.

(45) However, the actual distance between rcp and C−C bcp, which is inversely proportional to the strength of such topological interaction, is much larger in a NiC_2 rather than in a C_3 cycle.

(46) Collard, K.; Hall, G. G. *Int. J. Quantum Chem.* **1977**, *12*, 623−637.

(47) We have also searched for *intermolecular* critical points, which must verify the Morse equation, i.e., the Poincaré−Hopf rule for an extended system ($N - n + r - c = 0$, see: Johnson, C. K. *ACA Abstr. Ser. 2* **1992**, *29*, 105). All inversion centers are critical points (two rcp's, *e* and *b* in Wyckoff notation, and six bcp's) and 20 independent cp's (four rcp's and 16 bcp's) were also found in the regions of short H−H intermolecular interactions leading to a total of 25 intermolecular cp's (2/2 + 4 rcp's and 6/2 + 16 bcp's) in the asymmetric unit; no ccp could be located. The *cp*'s found do not comply the Morse relation (here, $N - n + r - c = -13$). Probably, this can be caused by the incorrect attribution of the signature for the Hessian matrix of the points where $\nabla\rho(\mathbf{r})$ vanishes, since $\rho(\mathbf{r})$ and its curvature are very small for all these contacts [$\rho(\mathbf{r_b}) < 0.05$ e Å^{-3}]. Moreover, some longer contacts may exhibit other cp's, while we have considered only H−H contacts smaller than 2.8 Å(further work is in progress to have a complete picture of the intermolecular interactions but the major *focus* here is on intramolecular bonding features).

Table 6. Electron Populations for Ni d-Orbitals (According to the Coordinate System Drawn in Chart **III**) and Atomic Charges, Grouped for Each *Pseudoequivalent Atom* (Model **3b**)

d-orbital populations		atomic charges		
			multipole refinement	Hirshfeld charge
total	7.91(3)	Ni	0.09(3)	+0.028
		C1	−0.25(3)	−0.05(2)
d(yz)	1.29(2)	C2	−0.26(3)	−0.054(11)
d(xz)	1.55(2)	C3	−0.28(5)	−0.11(3)
$d(x^2-y^2)$	1.60(2)	C4	−0.24(8)	−0.082(15)
$d(z^2)$	1.70(2)	$H(sp^2)$	0.26(1)	+0.10[a]
d(xy)	1.77(2)	$H(sp^3)$	0.12(1)	+0.06[a]

[a] For H atoms, we computed charges only for one $H(sp^2)$ and one $H(sp^3)$, thus these values are not averaged.

somewhat further advanced in the **c** to **d** transition than $(CO)_5W$-(C_2H_4).[48]

The emerging overall bonding picture agrees with the DCD model: both σ-donation and π-back-bonding are recognized in the Ni−C bond paths, which are inward pointing (σ-donation) but well apart and substantially close to Ni−C vectors (π-back-donation). σ-Donation emerges also from the decreased ellipticity of C1−C2 double bonds.

Atomic Populations and Charges. For transition metal atoms a partitioning scheme of d-electrons has been introduced[20a,49] and widely used whenever transition metal atoms have been studied. This partitioning relates d-electron density obtained from multipolar decomposition of experimental $\rho(\mathbf{r})$ with atomic d_i orbitals density. We applied it to the multipolar populations of Ni (model **3b**) and results are reported in Table 6.

We can apply the orbital picture emerged upon EHT computations for the interpretation of calculated orbital occupancies: indeed, d(*xz*) and d(*yz*), which were mainly responsible for back-donation effects, are the only two "depopulated" orbitals (as respect to an equipartion of the d^8s^2 configuration of Ni), while $d(z^2)$ and d(*xy*) are the most populated since they are involved in the ligand donation; having an undefined character, $d(x^2-y^2)$ is neither depopulated nor repopulated.

Besides the usage of monopole populations[50] (after multipole refinements), a different partitioning approach (the so-called *stockholder* method introduced by Hirshfeld[27]) can be used to estimate atomic charges: $\rho(\mathbf{r})$ at each point of the space is allocated to an atom in proportion to its contribution to the promolecule (IAM) at the same point. Atomic charges, evaluated either using monopole populations and Hirshfeld method, are reported in Table 6.

There is a close agreement between them: in particular, the small positive value computed for Ni indicates a slightly larger contribution of back-donation with respect to donation in M−L bonds. This is not surprising, since the COD ligand has much larger π-acid properties than, for instance, the ligand in ref 4f (where the Ni^{II} atom has a reduced positive charge, +0.9, due to σ-donation effects).

(48) A possible quantitative index for donor acceptor complex vs metallacycle dichotomy could also be the sum of the internal bp angles. In $Ni(COD)_2$ $\sum_{i=1}^{3}\beta_i \approx 113°$, in cyclopropane $\sum_{i=1}^{3}\beta_i \approx 237°$, while for a T-shaped complex, $\sum_{i=1}^{3}\beta_i \approx 0°$. However in refs 38 and 39 bond path angles are not reported, thus a comparison is not possible.

(49) Coppens, P. *The structure factor* in *International Tables for Crystallography*, Kluwer Academic Publisher: Dordrecht, 1995; Vol. B, pp 10−22.

(50) Coppens, P.; Guru Row, T. N.; Leung, P.; Stevens, E. D.; Becker, P. J.; Yang, Y. W. *Acta Crystallogr.* **1979**, *A35*, 63−72.

Conclusions

This paper reports the first complete topological analysis of a C═C double bond η^2-coordinated to a transition metal atom. In particular, the accurate ED of $Ni(COD)_2$ a *pseudo*tetrahedral species containing four η^2-coordinated C═C bonds has been determined.

A few experimental and methodological problems were addressed and solved, namely: (i) the collection strategy for the CCD area detector was optimized and its performances were monitored in order to obtain the required quality of data.[7] (ii) A "model independent" *qualitative* topology of $\rho(\mathbf{r})$ has been obtained by checking that different, but still meaningful, models were leading to the very same QTAM interpretation. (iii) The best (less redundant) model, which eventually resulted from the usage of "symmetry" restrained populations of the olefinic C atoms, has been extracted by careful physical (reasonable rigid bond test, electronic populations, and QTAM responses) and statistical tests.

The overall bonding picture emerging is in agreement with the DCD model: σ-donation and π-back-bonding are recognized in the Ni−C bond paths, which are *inwardly* curved (σ-donation) but well separated (π-back-donation). Topology speaks for a π-complex with a *concave* ring structure somewhat intermediate between a T-shape (which would imply a fully electrostatic model) and a *convex* ring (which would imply a fully covalent model). These results completely agree with those of previous *theoretical* QTAM studies on similar systems,[39] suggesting a mutual validation of the two approaches. It is also worth noting that the topological analysis of $\rho(\mathbf{r})$ (theoretically or experimentally determined) provided information that goes *beyond* a simple geometrical approach, which cannot address separately the two main bonding effects, or an orbitalic study, which cannot define a clear picture of the interactions (here represented by bond paths).[51]

As organometallic chemistry presents several kinds of bonds, lacking of a counterpart in the realm of organic molecules, we believe that more and more work should be directed toward a wide exploration of this field, which has been scarcely analyzed so far. In particular, as the CCD area detector allows fast (but still accurate) determination of charge density, we believe that QTAM analysis of *experimental* EDs will soon allow the *systematic* comparison of the different bonding capabilities of different ligands with an accuracy similar to that of *theoretical* QTAM studies.

Acknowledgment. We are thankful to Dr. L. Carlucci and to Dr. M. Bergamo for having crystallized with special care the air sensitive bis(1,5-cyclooctadiene)nickel, to Dr. T. Pilati for providing a powerful routine for molecular symmetrization, and to Professor R. Destro and Dr. N. Masciocchi for their comments on the manuscript. Professor R. Destro is thanked also for his continuos encouragement and for his experimental and theoretical support. P.M. dedicates this work to G. Poletti.

Supporting Information Available: Text describing a test of area-detector performances, Table A, a comparison of SMART CCD and Sintex P-1 data, table of coordinates and U_{iso} or U_{equiv} for $Ni(COD)_2$ after model **3b**, and a table of multipolar population parameters after refinement **3b** (11 pages). See any current masthead page for ordering information and Web access instructions.

JA972558L

(51) See Destro, R.; Merati, F. *Acta Crystallogr.* **1995**, *B51*, 559−570.